remote sensing

MDPI

Article

Ancient Burial Mounds Detection in the Altai Mountains with High-Resolution Satellite Images

Fen Chen [1,2,*], Lu Jin [2,3], Jean Bourgeois [4], Xiangguo Zuo [2], Tim Van de Voorde [5], Wouter Gheyle [4], Timo Balz [6] and Gino Caspari [7,8]

1 College of Computer Science, Chengdu University, No. 2025, Chengluo Avenue, Chengdu 610106, China
2 School of Resources and Environment, University of Electronic Science and Technology of China, 2006 Xiyuan Avenue, West Hi-Tech Zone, Chengdu 611731, China; 202122070309@std.uestc.edu.cn (L.J.); 202322070305@std.uestc.edu.cn (X.Z.)
3 Jiangxi Hongdu Aviation Industry Co., Ltd., Nanchang 330024, China
4 Department of Archaeology, Ghent University, Sint-Pietersnieuwstraat, 35, 9000 Ghent, Belgium; jean.bourgeois@ugent.be (J.B.); wouter.gheyle@west-vlaanderen.be (W.G.)
5 Department of Geography, Ghent University, Krijgslaan 281, S8, 9000 Ghent, Belgium; tim.vandevoorde@ugent.be
6 State Key Laboratory of Information Engineering in Surveying, Mapping and Remote Sensing, Wuhan University, Wuhan 430079, China; balz@whu.edu.cn
7 Domestication and Anthropogenic Evolution Research Group, Max Planck Institute of Geoanthropology, Kahlaische Str. 10, 07745 Jena, Germany; gino.caspari@gmail.com
8 Institute of Archaeological Sciences, University of Bern, Mittelstrasse 43, 3012 Bern, Switzerland
* Correspondence: chenfen@cdu.edu.cn

Highlights

What are the main findings?

- Deep learning techniques are applied for automatic kurgan identification.
- Performance of various CNN-based and Transformer-based object detection methods is comprehensively compared.

What is the implication of the main finding?

- Deep learning techniques are feasible for automatic kurgan identification.
- Deep learning techniques show strong potential for building a comprehensive inventory of kurgans in Altai Mountains.

Abstract

The Altai Mountains rank among the world's most notable and valuable archaeological regions. Within the sprawling Altai Mountains area, burial mounds (kurgans) of past civilizations, which are sometimes well preserved in permafrost, are a particularly precious trove of archaeological insights. This study investigates the application of deep learning-based object detection techniques for automatic kurgan identification in high-resolution satellite imagery. We compare the performance of various object detection methods utilizing both convolutional neural network and Transformer backbones. Our results validate the effectiveness of different approaches, especially with larger models, in the challenging task of detecting small archaeological structures. Techniques addressing the class imbalance can further improve performance of off-the-shelf methods. These findings demonstrate the feasibility of employing deep learning techniques to automate kurgan identification, which can improve archaeological surveying processes. It suggests the potential of deep learning technology for constructing a comprehensive inventory of Altai Mountain kurgans, particularly relevant in the context of global warming and archaeological site preservation.

Check for updates

Academic Editors: Timothy Murtha, Whittaker Schroder, Charles W Golden, Robert Griffin and Kelsey Herndon

Received: 27 August 2025
Revised: 13 October 2025
Accepted: 17 October 2025
Published: 6 January 2026

Copyright: © 2026 by the authors. Licensee MDPI, Basel, Switzerland. This article is an open access article distributed under the terms and conditions of the Creative Commons Attribution (CC BY) license.

Keywords: Altai mountains; ancient burial mound; global warming; remote sensing archaeology

1. Introduction

The Altai Mountains, spanning across Russia, Kazakhstan, China, and Mongolia in Central Asia and East Asia, constitute a highly impressive and valuable archaeological region. It is renowned for the remarkable archaeological significance of ethnically diverse nomadic tribes (e.g., Scythians, Huns, Turks) that once inhabited these regions from the Neolithic up to the Ethnographic period (from 4th millennium BCE to the 18th century CE).

The Altai Mountains region holds many traces of past civilizations, with the most notable being the tombs left by ancient nomadic pastoralist populations [1–3]. These burial mounds, known as kurgans, are an essential aspect of this region's cultural inheritance. They are valuable for archaeological research in Central and East Asia's cultural and societal understandings. Despite the decay of contents over time, leaving only bones and inorganic artefacts, some tombs are exceptionally well-preserved due to their remote location and unique geographical and climatic features. Located in the high altitudes, the Altai region goes through harsh climatic conditions with long winters, short summers, and low precipitation. Although such a climate may not be favorable for humans, it has been remarkably helpful in preserving fragile materials in tombs. In a few cases, the tombs are frozen by an ice lens of discontinuous permafrost below the stone mound. Therefore, parts of the most sensitive and interesting organic archaeological materials in these frozen tombs, such as textile and leather, which are more vulnerable than bones, metal, or stone objects, are remarkably well preserved [4–7]. These exceptional and invaluable materials provide valuable data for scientific purposes.

Kurgans represent the prevalent form of archaeological evidence in the Altai Mountains. They are scattered across the entire Altai landscape, from river valleys and terraces to high plateaus and ridge tops. They are built from piled-up stones, using both rough mountain rocks and smooth river cobbles. They are mostly round in form, and some of them have round or squared collars. Their diameter spans a great range, from mere meters to over 50 m. Their heights range from several meters to being nearly imperceptible against the ground. Kurgan distribution and arrangement in the Altai vary widely, with mounds appearing both in isolation and in groups. The burial traditions span an extensive period. For example, Early Iron Age kurgans are typically recognizable by their arrangement in north–south rows, a stark contrast to the Hunnic-Sarmatian period, where mounds were generally small, low and oval-shaped, and appear in clusters. Figure 1 shows a picture of the Scythian-era kurgans in the Altai Mountains.



Figure 1. Kurgans in the Altai Mountains.

Kurgans are always under threat from both natural disasters and human activities, such as earthquakes, floods, infrastructure construction, farmland activities, settlement expansion, and tourism. Among all these natural and anthropogenic threats, nowadays the most significant danger to these tombs arises from global warming. It hastens the rapidly melting permafrost, and this poses a considerable threat to the organic remains that have been well preserved in the tombs for more than two thousand years [2,8,9].

Although a few non-public atlases exist in the literature for several local regions [4–6,10], a detailed map of all the kurgans scattered in the whole Altai Mountains remains unavailable, which is a vital missing component for understanding past civilization in this region. Fieldwork is required to detailly map archaeological objects in local areas. However, such work is time-consuming, labor-intensive, and expensive. Furthermore, archaeological fieldwork is frequently hampered by political obstacles and the inaccessibility of extreme remote sites. Satellite imagery, however, can largely expand the scale and scope of archaeological surveys. Researchers have used high-resolution satellite imageries for visual identification of kurgans. For example, Balz et al. analyzed the discernibility of kurgans from TerraSAR-X data and discussed the limitations [11]. Caspari mapped the "royal" burial mounds and assessed their damages in the Siberian Valley of the Kings in the Tuva Republic with WorldView-2 data [12]. He also qualitatively assessed the recent looting state of Early Iron Age burial mounds in northern Xinjiang with both WorldView-2 and IKONOS images [13]. Vavulin et al. assessed the application potential and effectiveness of UAV-based photogrammetry for archaeological surveying in the Valley of the Kings [14]. Although UAV data can provide fine spatial resolution images for easy mapping, it is limitedly available in local regions, and fieldwork is still needed. High-resolution satellite images could be the sole data source for mapping large-scale areas. All these traditional methods of visual interpretation are not highly automated and were only evaluated in several small local areas. Therefore, it is still difficult to apply them to the mapping of kurgans scattered over the large Altai Mountains areas.

Over the last ten years, deep learning techniques, such as convolutional neural network (CNN), have significantly improved various computer vision applications [15–18]. In recent years, scholars have applied CNN-based techniques for the detection of kurgans. As an example, Caspari and Crespo used CNN to classify image subsets (100 × 100 pixels) from freely available Google Earth satellite imagery to determine whether an image subset contains kurgans or not [19]. They observed that the CNN-based classification approach outperformed the traditional support vector machine-based method. However, the used image classification method cannot precisely locate kurgans in the images. Chen et al. first used a CNN-based object detection method to automatically detect kurgans from high-resolution satellite images [20]. They demonstrated that, with the existing technological conditions, it is still difficult so far to achieve a high detection accuracy for kurgans from satellite images, because of both their small sizes and their low contrast with the background. However, they observed that the results obtained by the automatic CNN-based object detection method can already be useful for archaeologists, and the density map derived from the detection results corresponds well to the true spatial distribution of kurgans.

Transformer technique [21] has recently achieved great progress in the natural language processing (NLP) field, such as GPT-4 [22], and it has emerged to be one of the most attractive techniques in deep learning nowadays. Over the last few years, the Transformer technique has also demonstrated good potential in computer vision tasks [23] because of the advantage of capturing long-range dependencies much more effectively than a typical CNN. Inspired by the seminal work of Vision Transformer [24] that introduced the Transformer technique in image classification by treating an image as a sequence of small patches, Car-

ion et al. proposed the first fully end-to-end DEtection TRansformer (DETR) architecture by modeling object detection task as a problem of dictionary lookup with a set of learnable queries and achieved good results [25]. Despite exhibiting promising performance, DETR has slow training convergence and ambiguous query representation. Several methods have emerged to tackle these issues and to further improve the performance, including introducing deformable attention [26], providing spatial priors [27,28], introducing dynamic anchor boxes [29], and utilizing denoising techniques [30,31]. Swin Transformer [23] and Pyramid Vision Transformer [32] were proposed to utilize Transformer modular to build new backbones for network structure, which can serve as alternatives to traditional CNN backbones like ResNet [33], and ResNeXT [34], in various computer vision tasks. Although Transformer techniques have demonstrated better performance over CNNs in many NLP tasks in recent a few years, their efficacy in archaeological applications, particularly the detection of widely scattered small archaeological structures, remains to be rigorously validated to determine their potential advantage over CNNs.

In this study, we tested deep learning-based object detection technology to automatically identify kurgans from high-resolution satellite images on several kurgan sites that we have surveying data. Our results demonstrated that deep learning technique can be used to automate the detection of kurgans. We also applied this technique in two local unknown regions and discovered new kurgans there.

This paper is structured as follows: Section 2 describes the study sites and the image data. In Section 3, we detail the methodology of this study. The performance is evaluated and discussed in Sections 4 and 5, while Section 6 summarizes the conclusions.

2. Study Areas and Image Data

2.1. Study Sites

We selected study areas in several local regions for which we possess detailed field survey maps [14,35–41]. Figure 2 shows the locations of the study sites, with reference in the text. The locations feature various landscapes. For example, the valley of Karakol (site 1) is situated in lower parts of the Altai Mountains, at altitudes of about 1200 m and the presence of agricultural activities. The major Scyhtian tombs of Tuekta and Bashadar are part or close to this valley. These tombs resemble the monuments known from the so-called Valley of the kings in Tuva (site 2), that were also included in the dataset. The Yustid river (site 3) is located in a completely different landscape, characterized by a high steppe (1800–2000 m altitude) and no agricultural activity. The small Bar-Burgazy river is a tributary of Yustid river, running along the Turu Alty ridge. The southern edge of the Chuya steppe (site 4) is a study area with landscape conditions that are similar to those in Yustid, but with more closed valleys going higher up in the mountains. The Dzhazator valley (site 5) is a valley in more alpine conditions and forms one of the gateways to the important Ukok plateau on the borders with Russia, Kazakhstan, China and Mongolia. A comparable landscape can be found in the Bukhtarma valley (site 6) and surrounding region in Kazakhstan. In addition, we tested the proposed method in two more regions. One is near Dayan Lake, Bayan-Ölgii, Mongolia (site 7), where kurgans were reported in the literature [10]. Although kurgans were surveyed in this local region, the exact locations of these kurgans remain undisclosed to the archaeological community. The other region is in Heiliutan Basin, Xinjiang, China (site 8). In this area, we only have a small set of local field data [41], but it was expected that kurgans could exist in the other areas around it.

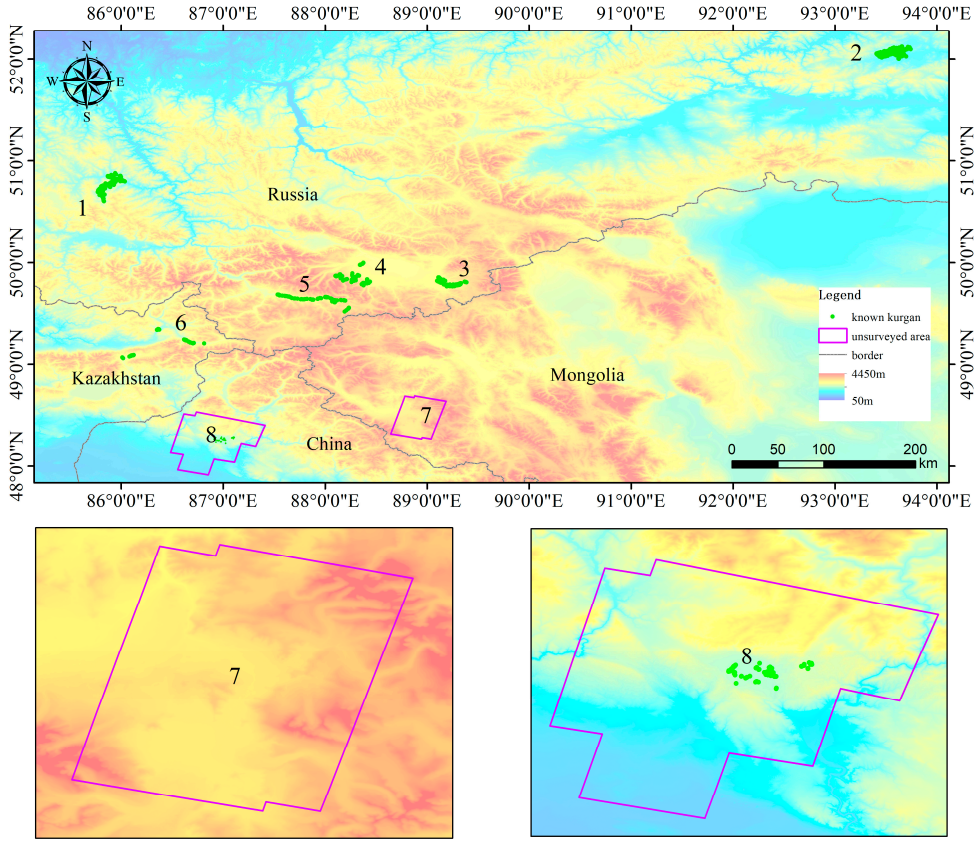


Figure 2. Study sites. Site 1: Valley of Karakol; Site 2: Valley of the kings; Site 3: Yustid river; Site 4: Chuya steppe; Site 5: Dzhazator valley; Site 6: Bukhtarma valley; Site 7: Dayan Lake; Site 8: Heiliutan Basin.

2.2. Image Data

In our study, we used Gaofen-2 (GF-2) satellite imagery, which originates from the satellite developed by China Academy of Space Technology and launched on 19 August 2014. It is a high-resolution optical Earth observation satellite primarily used for civilian applications. It has a panchromatic band with a ground sample distance (GSD) of 80 cm and four multispectral bands (red, green, blue, and near-infrared) with a GSD of 3.2 m. Each scene offers a swath of about 45 km. Note that, we pan-sharpened the multispectral data to an 80 cm spatial resolution with the panchromatic band using the Gram-Schmidt algorithm [42] in our experiments. Twenty-nine GF-2 images cover the six known areas, and eleven other GF-2 images cover the unknown Dayan Lake region and the Heiliutan Basin region. Note that, we selected the GF-2 data following a three-step prioritization process from the available archive, which provides multiple images across various years and seasons. First, we prioritized images recorded between May and October to avoid potential ice and snow coverage. Then, we selected images with minimal cloud cover to maximize the detection area. Finally, we opted to use the most recent images among the remaining options in order to show the kurgan's latest appearance.

One of the authors (L. Jin) created a dataset of samples of kurgans from the GF-2 satellite images that include all six known areas. The field data (shp file) was overlaid on the GF-2 satellite imagery for precise visual inspection. Only large mounds that are larger than 10 m were considered in our experiments, and only the clear ones were labeled. The reference data for each kurgan were carefully labeled with an open annotation tool (http://labelme.csail.mit.edu, accessed on 20 October 2025). For each kurgan, the bounding box around it was annotated. A total of 1087 sample images were obtained, each

with dimensions of 512 by 512 pixels. To enlarge the number of training samples, data augmentation techniques like flipping and zooming were employed.

3. Methodology

Machine-Learning Method

CNNs have emerged as dominant machine learning techniques, specifically within the realm of deep learning. They generally use shared-weight architecture of convolutional filters, which slide across input data and produce translation-equivariant feature maps. Hierarchical spatial feature extraction is achieved through successive convolutional layers, followed by pooling, fully connected, and normalization layers that refine these features for robust pattern recognition and classification.

Transformers are state-of-the-art deep learning architectures, which have now been used not only in NLP and computer vision, but also widely in other tasks like audio, multi-modal processing, and generative artificial intelligence, in which they have shown higher performance over CNNs. This technology is based on the attention mechanism [21]. Input information is first subdivided into tokens by a tokenizer, and each token is converted into a vector with its positional information embedded by an embedding layer. Then an encoder–decoder architecture is used for the Transformer module. The encoder layer employs a self-attention mechanism to generate context-aware token representations that mix information from different tokens. The decoder layer uses self-attention mechanisms to further refine these representations, allowing it to focus on relevant parts of the encoded information for generating the output. Fixed-size receptive fields limit CNNs, which restrict them to considering only a limited number of neighboring pixels at a time. In contrast, Transformers can capture long-range dependencies much more effectively, using context-based attention mechanisms.

In our implementation, we used the DDQ (Dense Distinct Query) object detection algorithm [43] with the Swin Transformer backbone network structure [23]. The Swin Transformer, like traditional Vision Transformers (ViT), breaks images into patches and processes them using a Transformer architecture. However, unlike traditional ViT which processes the entire image at once, Swin Transformer uses a shifted window approach. The image is divided into overlapping windows. Within each window, patches are processed using self-attention, a mechanism that helps the model identify relationships between image parts. These windows shift in subsequent layers, which allows the model to capture information across larger image regions while maintaining efficient computation. While Transformer-based algorithms like DETR use sparse queries, DDQ employs a dense grid of queries across the image, like traditional detectors. These dense queries ensure all potential objects have a chance of being detected. However, unlike traditional detectors, DDQ ensures these queries are distinct from each other. This helps the model to efficiently assign each object to a specific prediction, which leads to better overall optimization. As a result, DDQ can achieve higher recall compared to sparse query methods, which means it is more likely to detect all the objects in the image. Similarly to previous studies [44] that have used CNNs to classify small objects in large-scale satellite imagery, we found that prioritizing recall over precision is optimal as it takes a longer time to review imagery to identify missed detections rather than correcting false positive. Nevertheless, our dataset contains far fewer kurgan samples than background samples. To address this imbalance, we used the focal loss function [45] instead of the standard cross-entropy function during training. Focal loss is a variant of cross-entropy loss that dynamically adjusts the loss contribution of each example based on its confidence. Unlike traditional cross-entropy loss, which treats all examples equally, focal loss effectively reduces the influence of easily classified

examples, enabling the model to concentrate on more challenging instances during training and leading to more effective learning.

4. Experimental Results

All experiments were performed on a PC with a 3.7 GHz 6-core i7 CPU, 32 GB RAM, and an NVIDIA RTX 2080Ti graphics card. For the software implementation, the Pytorch-based MMDetection package v3.2.0 (https://github.com/open-mmlab/mmdetection, accessed on 20 October 2025) was used in our experiments. The models, which were pre-trained with the ImageNet dataset (https://image-net.org, accessed on 20 October 2025) and COCO dataset (https://cocodataset.org, accessed on 20 October 2025), were fine-tuned with our kurgan training samples.

The experimental workflow is summarized in Figure 3. The process began with the creation of labeled samples by cross-referencing satellite imagery from surveyed regions with field data. These labeled samples were then used to train kurgan detection models. Following training, the model's accuracy was evaluated. The validated model was subsequently applied to detect kurgans in satellite imagery of unknown regions. The final results were obtained following a visual inspection of these detections.

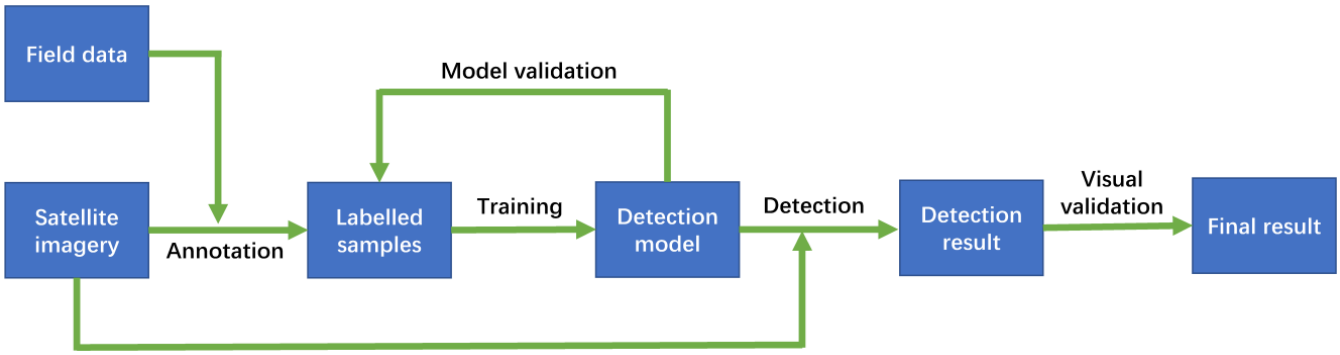


Figure 3. Flowchart of the experimental procedure.

We evaluated the performance using four-fold cross-validation with our collected kurgan dataset. The numbers of training, validation, and test datasets were divided with a split ratio of 4:1:1 at each round. The average performance was reported in the following. It is worth noting that utilizing a larger number of samples during training can generally enhance the accuracy of machine learning. Therefore, the entire set of sample images from the six known areas, which were used to collect kurgan samples, was employed to retrain the model specifically for the two unknown regions in the Dayan Lake area, Mongolia, and in the Heiliutan Basin area, China.

4.1. Accuracy Validation

We tested several commonly used object detection algorithms, including the Faster R-CNN algorithm [18], Cascade R-CNN algorithm [15], Deformable DETR [26], DINO algorithm [31], DDQ algorithm [43] for the kurgan detection task. In addition, we also compared various CNN-based network backbones and Transformer-based network backbones, which include ResNet-101 [33], ResNeXt-101 [34], PVT-2 [32], and Swin Transformer [23]. The cross-entropy (CE) function and the focal loss (FL) function [45] were also compared. Note that previously reported results [20] demonstrated that two-stage anchor-based object detection algorithms outperform both one-stage anchor-based and anchor-free methods. Because almost the same trend was observed in our experiments, we chose not to include the results of anchor-free and one-stage anchor-based methods in this paper.

The two commonly used metrics of AP and AR were adopted for the validation of performance for different models. The AP metric was used to evaluate the average precision of a model's detections across various levels of localization accuracy. The AR metric was used to summarize a model's performance of how well a model recalls or detects all instances of objects in an image for various localization accuracy. In our experiments for the unexplored regions, if a detected object has a confidence score larger than 0.5, it would be regarded as a kurgan. Therefore, in addition, the two metrics of Recall_{50} and Precision_{50}, which denote the recall and the precision at a confidence score threshold of 0.5, respectively, were both used to validate the performance of different algorithms. The F_β score, which is a weighted harmonic mean of precision and recall, was also used as a measure of detection performance. It considers recall is β times as important as precision. F_2 ($\beta = 2$) was used in our study as in [44].

As shown in Table 1, when the same object detection algorithm was used and the numbers of parameters (#param) in various backbone networks were similar, Transformer-based backbones achieved, in most cases, with only a few exceptions, comparable or better overall performance than CNN-based backbones. Among all the backbones, Swin-small used the fewest parameters but achieved comparable performance to larger CNN-based models, such as ResNet-101. For example, for the Faster R-CNN algorithm, the Swin-small model (#param = 45 M) achieved better results than the ResNet-101 model (#param = 60 M) in three metrics (AR, AP, Precision_{50}) with fewer parameters.

Since the performance of a model is correlated to the number of parameters, in general, the larger the size of a model, the better the performance is likely to be. Overall, it was observed that the Transformer-based PVT-v2 backbone obtained better results than the CNN-based ResNet-101, ResNeXt-101, and the Transformer-based Swin-small backbones. The better performance could be due to its large parameter size, which is the largest (#param $\approx$ 100 M) among the four. It was observed that, after upgrading the Swin Transformer model size from Swin-small to Swin-large, which had a parameter size larger than 200 M, the detection performance was improved for almost all tested object detection algorithms. For example, compared to the Swin-small model that had a parameter size of 73 M, by using the Swin-large model that had a parameter size of 241 M, the Cascade R-CNN algorithm obtained noticeable performance improvement (AR increased from 0.499 to 0.547, AP increased from 0.420 to 0.473, Precision_{50} increased from 0.737 to 0.798, F_2 increased from 0.762 to 0.775). A similar increase in performance was obtained for all the other algorithms.

Overall, the DDQ algorithm achieved better detection performance than the other algorithms when using the same network backbones, especially on recall performance. It means that the DDQ algorithm can detect more kurgans than the other algorithms while achieving comparable precision with them. For example, compared with all the tested approaches by using the same Swin-large model, the DDQ algorithm obtained the best recall performance (AR = 0.701, Recall_{50} = 0.826).

Due to the severe imbalance between the positive and negative samples in our dataset of kurgans, we also observed that using the focal loss function can effectively improve the detection accuracy of all object detection algorithms. For example, for the DDQ algorithm with the Swin-large backbone, all the four metrics appear to improve by using the focal loss function compared with the cross-entropy loss (AR increased from 0.701 to 0.804, AP increased from 0.523 to 0.681, Recall_{50} increased from 0.826 to 0.858, Precsion_{50} increased from 0.804 to 0.917, F_2 increased from 0.822 to 0.869). Focal loss tackles class imbalance by down-weighting easy negative samples. This allows the model to focus its learning on the more challenging positive examples, leading to improved model performance. This result indicates that if only a limited number of training samples can be obtained for targeted

small objects (not limited to kurgans, but also for other possible special small objects in other research fields), using techniques that consider the sample imbalance can effectively improve the detection performance.

From the numerical results presented in Table 1, it was observed that, among all the tested models, the DDQ object detection algorithm with both the Swin-large backbone network and the focal loss function performs the best. Therefore, in the following experiments, we used it as the kurgan detection model for the exploitation in the two unknown regions.

Table 1. Performance of different algorithms.

Algorithm	Backbone	Loss	#Param	AR	AP	$Recall_{50}$	$Precision_{50}$	F_2
Faster R-CNN	ResNet-101	CE	60 M	0.469	0.388	0.674	0.739	0.686
Faster R-CNN	ResNeXt-101	CE	60 M	0.490	0.418	0.708	0.787	0.723
Faster R-CNN	PVT-v2	CE	99 M	0.572	0.445	0.632	0.831	0.664
Faster R-CNN	Swin-small	CE	45 M	0.497	0.410	0.653	0.823	0.681
Faster R-CNN	Swin-large	CE	213 M	0.516	0.442	0.755	0.791	0.762
Faster R-CNN	Swin-large	FL	211 M	0.585	0.520	0.796	0.846	0.806
Cascade R-CNN	ResNet-101	CE	88 M	0.494	0.419	0.716	0.788	0.729
Cascade R-CNN	ResNeXt-101	CE	87 M	0.527	0.456	0.765	0.767	0.765
Cascade R-CNN	PVT-v2	CE	126 M	0.556	0.465	0.826	0.672	0.790
Cascade R-CNN	Swin-small	CE	73 M	0.499	0.420	0.768	0.737	0.762
Cascade R-CNN	Swin-large	CE	241 M	0.547	0.473	0.769	0.798	0.775
Cascade R-CNN	Swin-large	FL	238 M	0.734	0.546	0.828	0.901	0.842
Deformable DETR	ResNet-101	CE	59 M	0.572	0.390	0.676	0.795	0.697
Deformable DETR	ResNeXt-101	CE	54 M	0.528	0.315	0.538	0.795	0.575
Deformable DETR	PVT-v2	CE	94 M	0.628	0.351	0.705	0.805	0.723
Deformable DETR	Swin-small	CE	40 M	0.599	0.312	0.615	0.833	0.649
Deformable DETR	Swin-large	CE	208 M	0.606	0.327	0.635	0.849	0.669
Deformable DETR	Swin-large	FL	205 M	0.643	0.418	0.719	0.914	0.751
DINO	ResNet-101	CE	67 M	0.688	0.447	0.734	0.836	0.752
DINO	ResNeXt-101	CE	66 M	0.631	0.395	0.796	0.671	0.767
DINO	PVT-v2	CE	100 M	0.653	0.434	0.736	0.823	0.752
DINO	Swin-small	CE	48 M	0.682	0.493	0.751	0.830	0.766
DINO	Swin-large	CE	218 M	0.688	0.516	0.758	0.831	0.772
DINO	Swin-large	FL	215 M	0.788	0.583	0.825	0.867	0.833
DDQ	ResNet-101	CE	67 M	0.696	0.480	0.746	0.853	0.765
DDQ	ResNeXt-101	CE	62 M	0.687	0.435	0.736	0.814	0.750
DDQ	PVT-v2	CE	101 M	0.698	0.475	0.733	0.843	0.753
DDQ	Swin-small	CE	47 M	0.699	0.503	0.705	0.873	0.733
DDQ	Swin-large	CE	219 M	0.701	0.523	0.826	0.804	0.822
DDQ	Swin-large	FL	217 M	0.804	0.681	0.858	0.917	0.869

4.2. Discovering Kurgans in Unexplored Regions

To further assess the model's practical effectiveness in real-world situations in unexplored areas, we applied the model (DDQ algorithm with both Swin-large network backbone and focal loss function), which achieved the best performance on the collected kurgan dataset, on two regions with potential archaeological significance. One region is located near Dayan Lake, in western Mongolia's Bayan-Ölgii Province. The other region is in the Heiliutan Basin, Xinjiang, China. While archaeological literature [10,41] mention kurgans in these areas, their accurate geo-coordinates are still openly unavailable to the archaeological community. Note that, in the Heiliutan Basin area, we have a small set of local field data, which was obtained by Caspari in 2015. It was expected that kurgans could exist in the other areas around it. As this fieldwork in Heiliutan was carried out in 2015, we suppose that some of the recorded kurgans in the field data may have been destroyed due to newly built roads and some newly ploughed farmlands in this local area. The used

model was retrained with all the samples in the six known areas, which were used for model accuracy validation in the previous section (the field data in the Heiliutan being excluded in the training).

In the Dayan Lake region, we used four GF-2 satellite images covering an area of about 2000 km^2. In the Heiliutan Basin region, seven GF-2 images covering about 3200 km^2 were used. Details of these images are provided in the Supplementary Material (Table S1). Despite overlap among these images, we processed each satellite scene individually to identify kurgans. The results obtained from each scene were then combined with the non-maximum suppression (NMS) technique [46] to eliminate redundant detections. NMS helps refine our detections by removing kurgans with significant overlap with higher-scoring kurgans. In our experiments, we considered a kurgan redundant if its overlap with a higher-scoring kurgan exceeded a specified threshold (we used 0.5 in our experiments).

The used model yields promising results in these two unexplored areas, and the entire process only takes about 32 min and 55 min for the Dayan Lake and Heiliutan Basin, respectively. We successfully identified 315 and 427 objects in the Dayan Lake region and the Heiliutan Basin region, respectively. As a confirmation, one of the authors (J. Bourgeois, who is an archaeologist with more than 20 years of experience on Altai archaeological monuments) carefully checked these automatically identified kurgans, using Google Earth Pro v7.3. With a close visual inspection, beyond simply identifying a detected object as a kurgan or not, the archaeologist also cautiously assigned confidence levels to each result. In the manually checked results, 257 and 334 of these automatically detected objects are possible real kurgans (at different confidence levels) in the Dayan Lake area and the Heiliutan Basin area, respectively. Note that, in the 334 objects automatically identified in Heiliutan Basin, 49 were true kurgans after consulting the field data [41]. Figure 4 presents a zoomed view of the detection results in the Heiliutan Basin, overlaying them onto the field data. The largest mound identified by the used model in the Dayan Lake region has an estimated diameter of seventy-three meters, and the largest one in the Heiliutan Basin region has an estimated diameter of one hundred meters. Figure 5 shows some kurgans that were automatically detected by the used model in the two unexplored regions. This manual and visual check of the data also yielded wrongly detected objects. In the Dayan Lake area, fifty-eight objects were very unlikely to be kurgans, and ninety-three objects were also very unlikely to be kurgans in the Heiliutan Basin area. Certainly, field check is still crucial for definitive confirmation. Note that, ground-truthing complex, small objects in satellite imagery presents a significant challenge but necessary for fully validating image classification results. While experts can classify these images, on-the-ground confirmation is essential for complete validation. This issue is a common hurdle in many studies, including those focused on classifying small animals across large areas [47] and pastoralist surveys [44]. In remote regions, fieldwork is both expensive and logistically demanding, further complicating the validation process. Figure 6 shows the obtained kurgan results in the Dayan Lake and the Heiliutan Basin, respectively (Note that, objects appear overlaid due to the proximity among them). Figure 7 shows the density maps derived from them.

Alongside the determination of true kurgans and of wrongly detected objects by the automatic detection, the visual and manual analysis by an archaeologist using Google Earth images yielded a series of possible missed kurgans, i.e., objects that the archaeologist considers to likely be a kurgan. A total of 96 and 135 possible objects of that type were identified in the Dayan Lake and the Heiliutan Basin, respectively. Note that, in the 135 missed kurgans in the Heiliutan Basin, 46 were true kurgans after consulting the field data [41]. Certainly, the other possible missed kurgans need to be confirmed by future on-site investigations. We observe that these possible missed kurgans are all close to the results that were automatically identified by the used model. In the Dayan Lake region, all

the missed kurgans are within 2 km of the automatically detected ones. In the Heiliutan region among all the 135 missed kurgans, 113 (83.7%) are within 1 km of the detected ones, and 127 (94.1%) missed kurgans are within 2 km of the detected ones. The farthest missed kurgan is 3.9 km from the automatically detected kurgans. Note that, these missed ones are generally small kurgans. In addition, some of these missed kurgans were not very different from their surrounding areas in the used GF-2 satellite images, but they showed up more clearly against their backgrounds in the Google Earth images. Figure 8 illustrates some examples of such missed kurgans. Figure 8a shows mounds that were successfully detected by the used model in the GF-2 scene. In Figure 8b which shows the corresponding Google Earth images, a few smaller kurgans were observed to be missed by the used model. One can see that these missed mounds showed up more clearly against their backgrounds in the Google Earth image than in the GF-2 images. This phenomenon could be due to two reasons. First, the Google Earth image and the GF-2 image were recorded at different times. In this small local area, the Google Earth image was recorded in October 2012, and the GF-2 image was recorded in August 2020. Some kurgans could be destroyed in recent years due to human activities. In addition, vegetation may obscure some stones seasonally. Second, the satellite sensors' characteristics are different. The quality of Google Earth images in this local region seems to be better than the used GF-2 images.

It should be noted that the validation work executed in the two unexplored regions was based mainly on visual inspection instead of field verification. While this method provides a preliminary assessment of the results, these findings require further confirmation. Therefore, we plan to formally validate these detection results in the future, ideally through in situ surveys conducted by the research team or by establishing collaborations with local institutions that possess regional expertise and access to these remote areas.

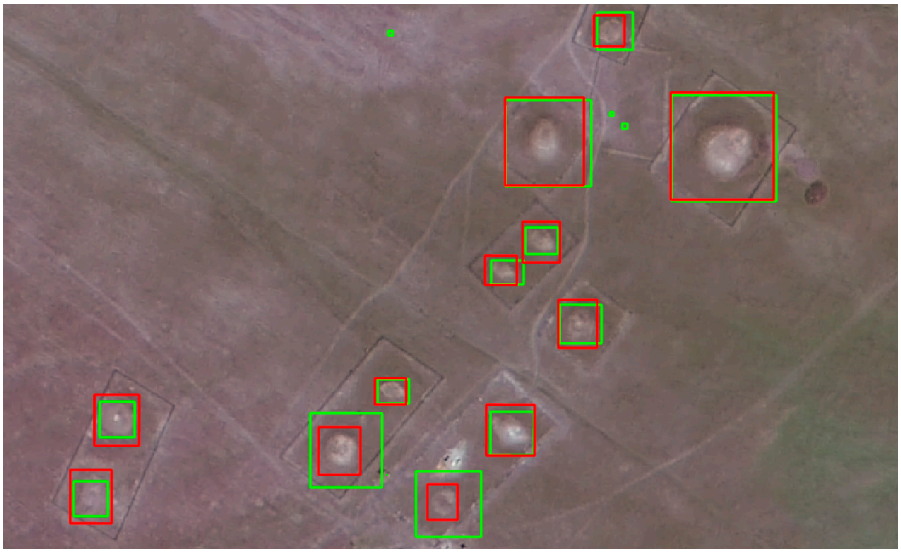


Figure 4. Zoomed-in view of the detected kurgans in the Heiliutan Basin. The field data is outlined by the green box, and the detection results are shown in red.

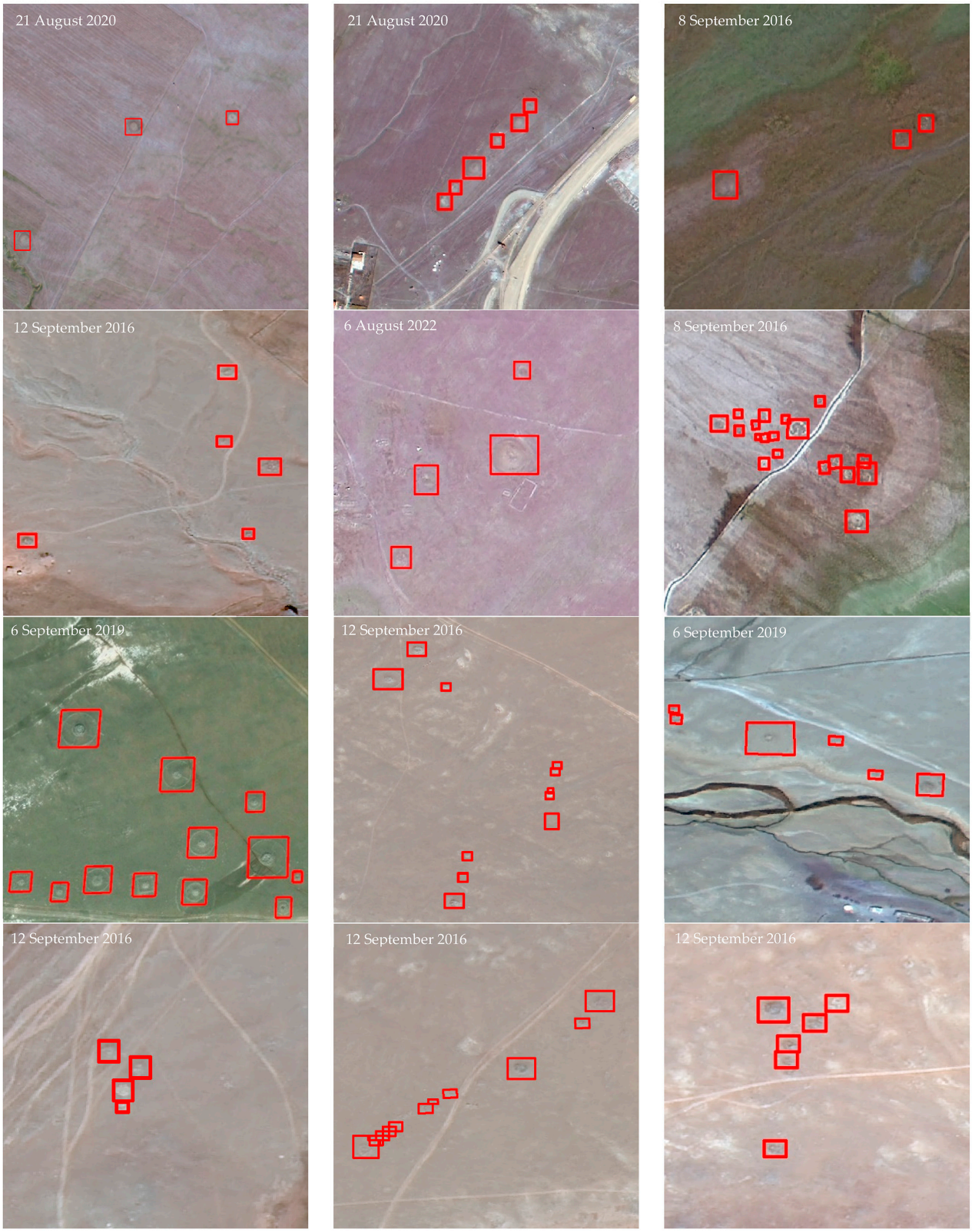


Figure 5. Detected kurgans in the two unexplored regions from GF-2 satellite images. Note that, for a neater presentation, these sub-images were uniformly zoomed to the same size.

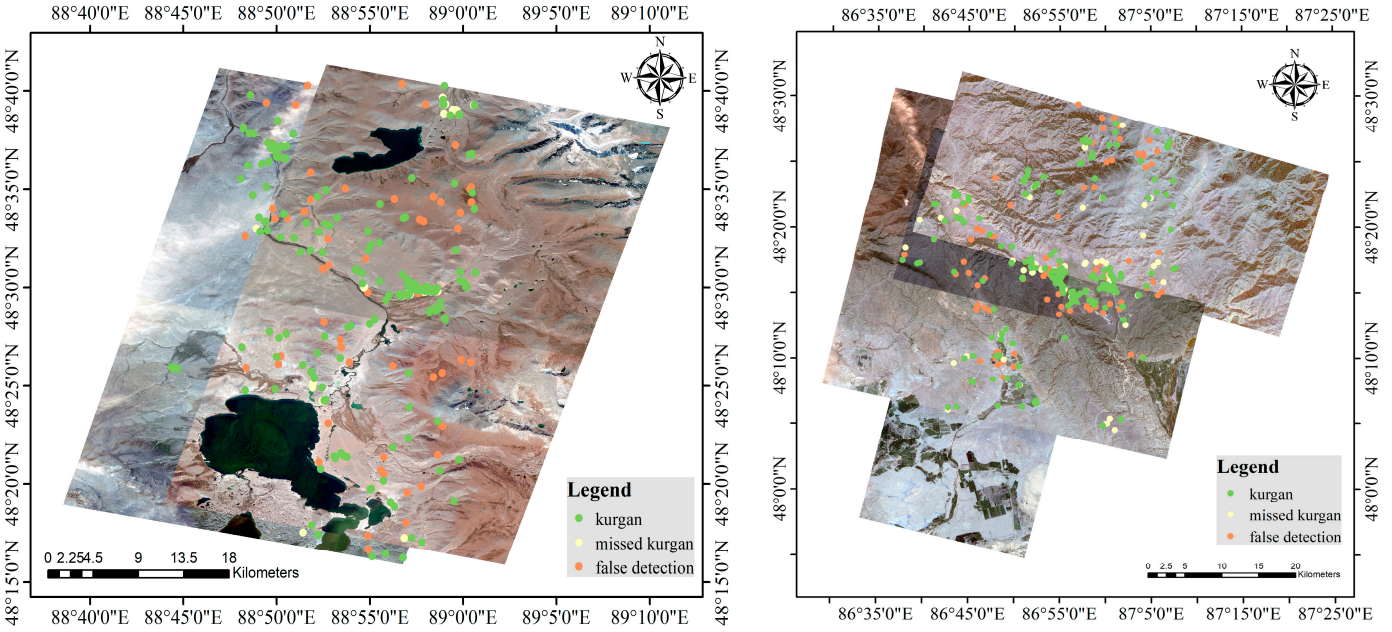


Figure 6. Results in the two unexplored regions. (**a**) Dayan Lake, Bayan-Ölgii, Mongolia; (**b**) Heiliutan Basin, Xinjiang, China. Note that, for a neater presentation, sub-images were uniformly zoomed to the same height.

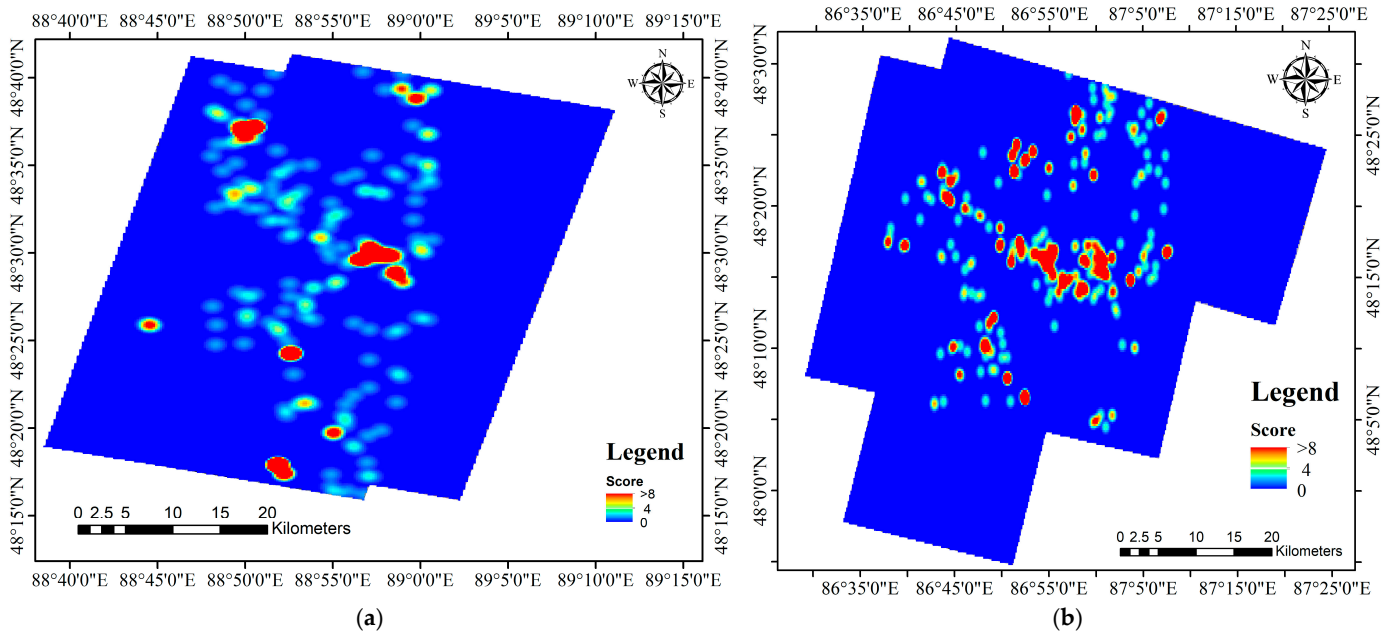


Figure 7. Derived density map from the detection results in the two unexplored regions. (**a**) Dayan Lake, Bayan-Ölgii, Mongolia; (**b**) Heiliutan Basin, Xinjiang, China. in Dayan Lake, Mongolia. Note that, for a neater presentation, sub-images were uniformly zoomed to the same height.

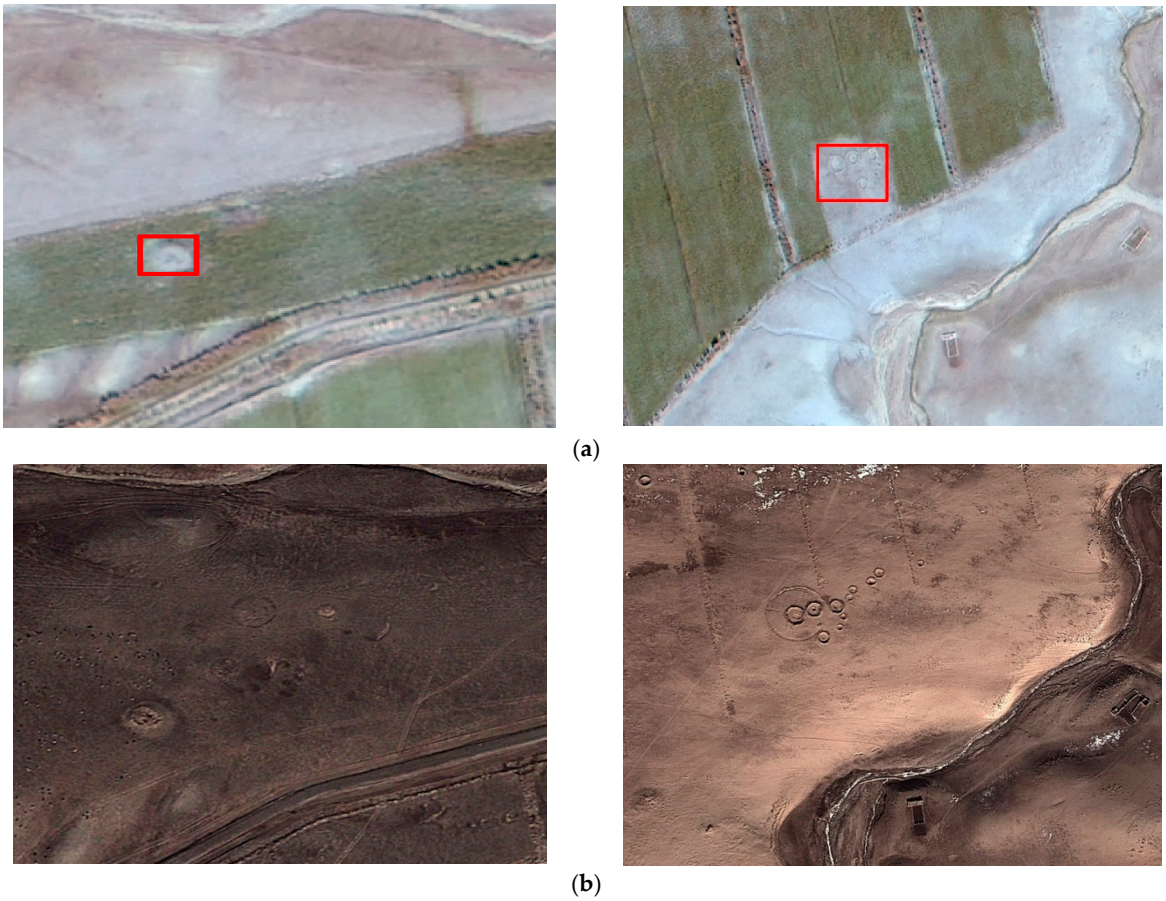


Figure 8. Kurgans shown in different satellite scenes. (**a**) GF-2 image in Aug. 2020; (**b**) Image@ [October 2012] Google Earth, Maxar Technologies.

5. Discussion

From our above experimental results, we observe that the Transformer technique outperformed CNN in kurgan detection, and the detection performance increases with the model size. It indicates that Transformer is a valuable new technique that has the potential to be applied to the kurgan detection task in the whole Altai Mountains. Note that this study aims to evaluate the feasibility of the deep learning technique in kurgan detection. We only tested those commonly used (relatively small) models due to the limited memory of the used GPU and compared those models with similar or comparable parameter sizes. Given Transformers' ability to manage larger model sizes more efficiently than CNNs, we anticipate significant performance improvements by deploying bigger models and leveraging more training data in the future. Historically, the evaluation of deep learning-based object detection methods has predominantly relied on precision as the primary accuracy metric for detection performance. Different from this traditional view, in this study, we have gained this insight from our experiences that finding mistakes in the detected objects (false positives) is much easier than identifying missed kurgans (false negatives) during the final visual checks. False positives require a simple mouse/keyboard click to remove, while false negatives demand a meticulous, time-consuming search of the entire scene. Therefore, from a practical viewpoint, we consider prioritizing high recall (finding most kurgans) is more important than high precision (avoiding mistakes) in kurgan detection. A high recall rate but low precision will still likely create extra costs for archaeologists. To mitigate this, some additional approaches, such as incorporating prior knowledge of archaeology, using multi-temporal analysis, could be applied before a final manual review.

Although the Transformer outperforms CNN and can detect most of the kurgans in unknown areas, it was observed that there were still some missed kurgans and false detections in the results. Several factors can contribute to missed kurgans, including the characteristics of used satellite imagery (e.g., spatial resolution, radiometric resolution, image contrast), the size of kurgans, and image acquisition timing. For example, despite using 80 cm high-resolution satellite imagery, the spatial resolution still is inadequate to detect some smaller kurgans, which only occupy a few pixels in the images. Using data with finer spatial resolution, such as UAV imagery, could be better. Additionally, integrating SAR data, which offers complementary characteristics distinct from optical satellite imagery, presents another possible way. Some kurgans cannot be easily distinguished from their surrounding backgrounds at certain times because their subtle features are masked by environmental factors, but they could become easier to see at another time when those conditions change. Using multi-temporal data may provide information that can be used to address this issue. Leveraging the inherent diversity of spectral and spatial characteristics across different satellite sensors may yield a synergistic effect to enable the identification of more kurgans within a scene compared to utilizing data from a single source. The main reason for false detections is due to that there are features in satellite imagery that exhibit similarities to kurgans. Some human features and vegetation features in the Altai Mountains demonstrate very similar characteristics to kurgans in the satellite images, leading to misidentification. It might be impossible to eradicate these false detections solely with satellite data. Although trained archaeologists can remove a part of them by visual check of the satellite imagery, they are still not fully confident about the others. Fieldwork is still required to confirm whether they are kurgans or not. It is important to note that the limitations of current object detection algorithms, which are not yet fully optimized for landscape archaeology, contribute to both missed kurgans and false detections. However, advancements in technology are anticipated to enhance the accuracy of kurgan detection in the future. Although the eight selected study sites represent some typical landscapes, they are insufficient to fully capture the vast diversity inherent in the Altai Mountains' geomorphological complexity. Therefore, developing a more practical kurgan detection model applicable to the entire Altai region necessitates incorporating a broader range of diverse landscapes into the training dataset. The integration of typical background image samples into the training procedure has been shown to enhance detection precision [20].

Instead of a time-consuming visual search in every location, by using our method, archaeologists can efficiently remove most false detections and identify missed kurgans with quick visual checks in just a few targeted key areas. This significantly reduces the archaeologists' workload and helps to create a preliminary list of monuments in not yet surveyed regions, which can guide future field control expeditions.

Concerning the dating of the automatically detected kurgans from satellite images, some formal and spatial characteristics can be used. For example, a cluster of Scythian mounds demonstrates a North–South oriented linear structure, and some collared mounds and kereksur have characteristic collars, fences, or spokes [48,49]. However, top-view satellite data alone is insufficient for archaeologists to date the other sites. We need more information in these cases, and this information obviously has to be further collected through fieldwork and archaeological research.

6. Conclusions

This study explored the application of deep learning-based object detection for automatic kurgan identification in high-resolution satellite imagery of the Altai Mountains, a region rich in archaeological treasures. Our findings validate the enhanced performance of Transformer-based methods, particularly with larger models, over traditional CNN

approaches in the challenging task of detecting small archaeological structures. Moreover, the application of class imbalance mitigation techniques significantly improves the kurgan detection performance of standard object detection methods, particularly when applied to datasets that deviate from typical daily-life object distributions. Given the specific challenges associated with detecting small and often subtle archaeological structures, our research indicates the necessity of prioritizing recall over precision. Note that these findings apply more broadly to the detection of other small cryptic objects in satellite imagery.

Our results suggest the immense potential of constructing a comprehensive kurgan inventory across the Altai Mountains. To further advance this research, future work could involve scaling up the models to allow for more comprehensive analyses and employing more powerful computing infrastructure to enable faster training and inference, thus accelerating the pace of discovery. Additionally, extending these techniques to diverse archaeological contexts in other geographical regions of the world is essential to unlocking the full potential of artificial intelligence in landscape archaeology.

Supplementary Materials: The following supporting information can be downloaded at: https://www.mdpi.com/article/10.3390/rs18020185/s1.

Author Contributions: Conceptualization, F.C.; Methodology, F.C., L.J., J.B., T.V.d.V. and W.G.; Software, F.C., L.J. and X.Z.; Validation, F.C., L.J., J.B., X.Z., T.V.d.V., W.G. and G.C.; Formal analysis, F.C., L.J., J.B. and X.Z.; Investigation, F.C.; Resources, F.C.; Data curation, F.C., L.J. and X.Z.; Writing—original draft, F.C.; Writing—review and editing, F.C., J.B., T.V.d.V., W.G., T.B. and G.C.; Visualization, L.J. and W.G.; Supervision, F.C.; Project administration, F.C.; Funding acquisition, F.C. All authors have read and agreed to the published version of the manuscript.

Funding: This work was supported by the National Science Foundation of China under Grant 42171334, and in part by the Chinese Academy of Sciences President's International Fellowship Initiative under Grant 2024PVB0064 and the Dragon-6 project under Grant 95387.

Data Availability Statement: The data that support the findings of this study are available from the corresponding author upon reasonable request.

Conflicts of Interest: Author L.J. is employed by Jiangxi Hongdu Aviation Industry Co., Ltd. The remaining authors declare that the research was conducted in the absence of any commercial or financial relationships that could be construed as a potential conflict of interest.

References

1. Baumer, C. *The History of Central Asia: The Age of the Steppe Warriors*; I.B. Tauris & Co., Ltd.: London, UK; New York, NY, USA, 2012.
2. Han, J.; Frank, L.; Treselian, D. (Eds.) *The Preservation of the Frozen Tombs of the Altai Mountains*; UNESCO World Heritage Centre: Paris, France, 2008.
3. Rudenko, S.I.; Thompson, M.W. *Frozen Tombs of Siberia: The Pazyryk Burials of Iron-Age Horsemen*; J.M. Dent & Sons Ltd.: London, UK, 1970.
4. Kubarev, V.D. *Курганы Уландрыка—Kurgany Ulandryka*; Наука: Новосибирск, Russia, 1987.
5. Kubarev, V.D. *Курганы Юстыда—Kurgany Yustyda*; Наука: Новосибирск, Russia, 1991.
6. Kubarev, V.D. *Курганы Сайлюгема—Kurgany Saylyugema*; Наука: Новосибирск, Russia, 1992.
7. Čugunov, K.V.; Parzinger, H.; Nagler, A. *Der Goldschatz von Arzan: Ein Fürstengrab der Skythenzeit in der Südsibirischen Steppe*; Schirmer/Mosel: München, Germany, 2006.
8. Bourgeois, J.; De Wulf, A.; Goossens, R.; Gheyle, W. Saving the frozen Scythian tombs of the Altai Mountains (Central Asia). *World Archaeol.* **2007**, *39*, 458–474. [CrossRef]
9. Bourgeois, J.; Gheyle, W.; Babin, V.; Lukyanenko, V.N. The frozen tombs of the Altay Mountains: Strategies and perspectives. In Proceedings of the UNESCO Workshop, Gorno-Altaisk, Russia, 28–31 March 2006; UNESCO/Flanders Funds-in-Trust. Gorno-Altaisk State University: Gorno-Altaisk, Russia, 2007.
10. Jacobson-Tepfer, E.; Meacham, J.E. *Archaeology and Landscape in the Mongolian Altai: An Atlas*; ESRI Press: Redlands, CA, USA, 2009.
11. Balz, T.; Caspari, G.; Fu, B.; Liao, M. Discernibility of burial mounds in high-resolution X-Band SAR images for archaeological prospections in the Altai Mountains. *Remote Sens.* **2016**, *8*, 817. [CrossRef]

12. Caspari, G. Mapping and damage assessment of "royal" burial mounds in the Siberian Valley of the Kings. *Remote Sens.* **2020**, *12*, 773. [CrossRef]
13. Caspari, G. Assessing looting from space: The destruction of Early Iron Age burials in northern Xinjiang. *Heritage* **2018**, *1*, 21. [CrossRef]
14. Vavulin, M.V.; Chugunov, K.V.; Zaitceva, O.V.; Vodyasov, E.V.; Pushkarev, A.A. UAV-based photogrammetry: Assessing the application potential and effectiveness for archaeological monitoring and surveying in the research on the 'valley of the kings' (Tuva, Russia). *Digit. Appl. Archaeol. Cult. Herit.* **2021**, *20*, e00172. [CrossRef]
15. Cai, Z.; Vasconcelos, N. Cascade R-CNN: Delving into high quality object detection. In Proceedings of the IEEE Conference on Computer Vision and Pattern Recognition, Salt Lake City, UT, USA, 18–23 June 2018; pp. 6154–6162.
16. Chen, F.; Zhao, H.; Roberts, D.; Van de Voorde, T.; Batelaan, O.; Fan, T.; Xu, W. Mapping center pivot irrigation systems in global arid regions using instance segmentation and analyzing their spatial relationship with freshwater resources. *Remote Sens. Environ.* **2023**, *297*, 113760. [CrossRef]
17. He, K.; Gkioxari, G.; Dollár, P.; Girshick, R. Mask R-CNN. In Proceedings of the IEEE International Conference on Computer Vision, Venice, Italy, 22–29 October 2017; pp. 2980–2988.
18. Ren, S.; He, K.; Girshick, R.; Sun, J. Faster R-CNN: Towards real-time object detection with region proposal networks. *IEEE Trans. Pattern Anal. Mach. Intell.* **2017**, *39*, 1137–1149. [CrossRef]
19. Caspari, G.; Crespo, P. Convolutional neural networks for archaeological site detection—Finding 'Princely' tombs. *J. Archaeol. Sci.* **2019**, *110*, 104998. [CrossRef]
20. Chen, F.; Zhou, R.; Van de Voorde, T.; Chen, X.; Bourgeois, J.; Gheyle, W.; Goossens, R.; Yang, J.; Xu, W. Automatic detection of burial mounds (kurgans) in the Altai Mountains. *ISPRS J. Photogramm. Remote Sens.* **2021**, *177*, 217–237. [CrossRef]
21. Vaswani, A.; Shazeer, N.; Parmar, N.; Uszkoreit, J.; Jones, L.; Gomez, A.N.; Kaiser, Ł.; Polosukhin, I. Attention is all you need. In Proceedings of the Advances in Neural Information Processing Systems, Long Beach, CA, USA, 4–9 December 2017; p. 30.
22. OpenAI GPT-4 Technical Report. *arXiv* **2023**, arXiv:2303.08774v3.
23. Liu, Z.; Lin, Y.; Cao, Y.; Hu, H.; Wei, Y.; Zhang, Z.; Lin, S.; Guo, B. Swin transformer: Hierarchical vision transformer using shifted windows. In Proceedings of the IEEE International Conference on Computer Vision, Montreal, BC, Canada, 11–17 October 2021; pp. 10012–10022.
24. Dosovitskiy, A.; Beyer, L.; Kolesnikov, A.; Weissenborn, D.; Zhai, X.; Unterthiner, T.; Dehghani, M.; Minderer, M.; Heigold, G.; Gelly, S.; et al. An image is worth 16x16 words: Transformers for image recognition at scale. *arXiv* **2020**, arXiv:2010.11929.
25. Carion, N.; Massa, F.; Synnaeve, G.; Usunier, N.; Kirillov, A.; Zagoruyko, S. End-to-end object detection with transformers. In Proceedings of the European Conference on Computer Vision, Glasgow, UK, 23–28 August 2020; pp. 213–229.
26. Zhu, X.; Su, W.; Lu, L.; Li, B.; Wang, X.; Dai, J. Deformable DETR: Deformable transformers for end-to-end object detection. *arXiv* **2020**, arXiv:2010.04159.
27. Gao, P.; Zheng, M.; Wang, X.; Dai, J.; Li, H. Fast convergence of DETR with spatially modulated co-attention. In Proceedings of the IEEE International Conference on Computer Vision, Montreal, BC, Canada, 11–17 October 2021; pp. 3621–3630.
28. Yao, Z.; Ai, J.; Li, B.; Zhang, C. Efficient DETR: Improving end-to-end object detector with dense prior. *arXiv* **2021**, arXiv:2104.01318.
29. Liu, S.; Li, F.; Zhang, H.; Yang, X.; Qi, X.; Su, H.; Zhu, J.; Zhang, L. Dab-DETR: Dynamic anchor boxes are better queries for DETR. *arXiv* **2022**, arXiv:2201.12329. [CrossRef]
30. Li, F.; Zhang, H.; Liu, S.; Guo, J.; Ni, L.M.; Zhang, L. DN-DETR: Accelerate DETR training by introducing query denoising. In Proceedings of the IEEE Conference on Computer Vision and Pattern Recognition, New Orleans, LA, USA, 18–24 June 2022; pp. 13619–13627.
31. Zhang, H.; Li, F.; Liu, S.; Zhang, L.; Su, H.; Zhu, J.; Ni, L.M.; Shum, H.Y. Dino: DETR with improved denoising anchor boxes for end-to-end object detection. *arXiv* **2022**, arXiv:2203.03605.
32. Wang, W.; Xie, E.; Li, X.; Fan, D.P.; Song, K.; Liang, D.; Lu, T.; Luo, P.; Shao, L. Pvt v2: Improved baselines with pyramid vision transformer. *Comput. Vis. Media* **2022**, *8*, 415–424. [CrossRef]
33. He, K.; Zhang, X.; Ren, S.; Sun, J. Deep residual learning for image recognition. In Proceedings of the IEEE Conference on Computer Vision and Pattern Recognition, Las Vegas, NV, USA, 27–30 June 2016; pp. 770–778.
34. Xie, S.; Girshick, R.; Dollár, P.; Tu, Z.; He, K. Aggregated residual transformations for deep neural networks. In Proceedings of the IEEE Conference on Computer Vision and Pattern Recognition, Honolulu, HI, USA, 21–26 July 2017; pp. 1492–1500.
35. Bourgeois, J.; De Wulf, A.; Ebel, A.V.; Gheyle, W.; Goossens, R.; van Hoof, L. Mapping and surveying the archaeological monuments of the Altai Mountains (Altai Republic). In Proceedings of the 34th Conference Computer Applications and Quantitative Methods in Archaeology, Dublin, Ireland, 18–21 April 2006.
36. Bourgeois, J.; Gheyle, W.; Goossens, R.; Van de Kerchove, R.; Dvornikov, E.P.; Ebel, A.V.; van Hoof, L.; De Wulf, A.; Loute, S.; De Langhe, K.; et al. Survey and inventory of the archaeological sites in the valley of the Karakol (Uch-Enmek Park): Report on the Belgian-Russian Expedition in the Russian Altay Mountains 2007–2008. *Mir Evrazii* **2009**, *1*, 10–20.

37. Bourgeois, J.; Cheremisin, D.V.; Plets, G.; Dvornikov, E.P.; Ebel, A.V.; Stichelbaut, B.; Van Hoof, L.; Gheyle, W. An archaeological landscape in the Dzhazator valley (Altai Mountains): Surface monuments and petroglyphs from the Chalcolithic to the Ethnographic period. *Archaeol. Ethnol. Anthropol. Eurasia* **2014**, *42*, 106–119. [CrossRef]
38. Gheyle, W.; Trommelmans, R.; Bourgeois, J.; Goossens, R.; Bourgeois, I.; De Wulf, A.; Willems, T. Evaluating CORONA: A case study in the Altai Republic (South Siberia). *Antiquity* **2004**, *78*, 391–403. [CrossRef]
39. Gheyle, W.; De Wulf, A.; Dvornikov, E.P.; Ebel, A.V.; Goossens, R.; Bourgeois, J. Early Iron Age burial mounds in the Altay Mountains—From survey to analysis. In *Tumulus as Sema: Space, Politics, Culture and Religion in the First Millennium BC*; Henry, O., Kelp, U., Eds.; De Gruyter: Berlin, Germany, 2016.
40. Goossens, R.; De Wulf, A.; Bourgeois, J.; Gheyle, W.; Willems, T. Satellite imagery and archaeology: The example of CORONA in the Altai Mountains. *J. Archaeol. Sci.* **2006**, *33*, 745–755. [CrossRef]
41. Caspari, G.; Plets, G.; Balz, T.; Fu, B. Landscape archaeology in the Chinese Altai Mountains–Survey of the Heiliutan Basin. *Archaeol. Res. Asia* **2017**, *10*, 48–53. [CrossRef]
42. Laben, C.A.; Brower, B.V. Process for Enhancing the Spatial Resolution of Multispectral Imagery Using Pan-Sharpening. U.S. Patent 6011875, 4 January 2000.
43. Zhang, S.; Wang, X.; Wang, J.; Pang, J.; Lyu, C.; Zhang, W.; Luo, P.; Chen, K. Dense distinct query for end-to-end object detection. In Proceedings of the IEEE Conference on Computer Vision and Pattern Recognition, Vancouver, BC, Canada, 17–24 June 2023; pp. 7329–7338.
44. Duporge, I.; Isupova, O.; Reece, S.; Macdonald, D.W.; Wang, T. Using very-high-resolution satellite imagery and deep learning to detect and count African elephants in heterogeneous landscapes. *Remote Sens. Ecol. Conserv.* **2021**, *7*, 369–381. [CrossRef]
45. Lin, T.; Goyal, P.; Girshick, R.B.; He, K.; Dollár, P. Focal loss for dense object detection. In Proceedings of the IEEE International Conference on Computer Vision, Venice, Italy, 22–29 October 2017; pp. 2999–3007.
46. Girshick, R.; Donahue, J.; Darrell, T.; Malik, J. Rich feature hierarchies for accurate object detection and semantic segmentation. In Proceedings of the IEEE Conference on Computer Vision and Pattern Recognition, Columbus, OH, USA, 23–28 June 2014; pp. 580–587.
47. Wu, Z.; Zhang, C.; Gu, X.; Duporge, I.; Hughey, L.F.; Stabach, J.A.; Skidmore, A.K.; Hopcraft, J.G.C.; Lee, S.J.; Atkinson, P.M.; et al. Deep learning enables satellite-based monitoring of large populations of terrestrial mammals across heterogeneous landscape. *Nat. Commun.* **2023**, *14*, 3072. [CrossRef]
48. Bourgeois, J.; De Langhe, K.; Ebel, A.V.; Dvornikov, E.P.; Konstantinov, N.A.; Gheyle, W. Geometric stone settings in the Yustyd valley and its surroundings (Altai Mountains, Russia): Bronze age 'virtual dwellings' and associated structures. *Archaeol. Res. Asia* **2017**, *10*, 17–31. [CrossRef]
49. Gheyle, W. Highlands and Steppes: An Analysis of the Changing Archaeological Landscape of the Altay Mountains from the Eneolithic to the Ethnographic Period. Ph.D. Thesis, Ghent University, Gent, Belgium, 2009.

Disclaimer/Publisher's Note: The statements, opinions and data contained in all publications are solely those of the individual author(s) and contributor(s) and not of MDPI and/or the editor(s). MDPI and/or the editor(s) disclaim responsibility for any injury to people or property resulting from any ideas, methods, instructions or products referred to in the content.